Semiconductor Physics, Quantum Electronics & Optoelectronics, 2025. V. 28, No 4. P. 456-463.

Optics

Raman study of structural changes in Si-based materials induced by scanning with IR ns-pulsed laser

V.M. Dzhagan[1], P.M. Lytvyn[1], A.A. Korchovyi[1], V.O. Yukhymchuk[1], V.V. Strelchuk[1], K.V. Svezhentsova[1], G.M. Androsyuk[1], O.V. Dubikovsky[1], V.V. Dzhahan[2], S.V. Kondratenko[2]

[1] *V. Lashkaryov Institute of Semiconductor Physics, NAS of Ukraine, 41, Nauky ave., 03028 Kyiv, Ukraine*
[2] *Physics Department, Taras Shevchenko National University of Kyiv, Kyiv, Ukraine*
[*] *Corresponding author e-mail: dzhagan@isp.kiev.ua*

Abstract. With the increasing availability of scanning laser systems and direct laser writing and lithography equipment, investigations of laser modification of materials regain their high relevance for both emerging and well-established semiconductors, such as Si. In this work, we have used Raman spectroscopy to study the structural modification of amorphous Si (a-Si), polycrystalline Si (poly-Si), Si nanocrystals embedded in SiO_2-matrix (ncSi-SiO_2), as well as SiO_2/Si/SiO_2 multilayer structures, subjected to 1064 nm pulsed laser annealing (PLA) by a commercial scanning laser (engraver). Raman scattering spectroscopy was used as the main technique for studying the induced structural changes due to the high sensitivity of phonon peak parameters to structural disorder and lattice strain. Comparison of the spectra measured at different excitation wavelengths allows one to probe the annealed structures at various depths. For a-Si, the PLA induces local formation of highly crystalline Si patterns. The process exhibits a threshold effect, with qualitative changes in the spectrum measured for samples annealed at 2-3% change in the PLA power. For a set of SiO_2/Si/SiO_2 multilayers with different combinations of layer thickness, PLA results in a relaxation to a state that no longer depends on the thicknesses of the Si and SiO_2 layers.

Keywords: laser annealing, amorphous silicon, polycrystalline silicon, Si nanocrystals.

https://doi.org/10.15407/spqeo28.04.456
PACS 42.65.Dr, 61.80.Ba, 78.30.Am, 78.30.Fs

Manuscript received 02.08.25; revised version received 21.10.25; accepted for publication 26.11.25; published online 15.12.25.

1. Introduction

Along with the emergence of numerous new materials, silicon remains the prevailing material in micro- and nano-electronics and photonics [1–3]. Moreover, in the search for new materials for electronics, optoelectronics, and sensors, their compatibility with established Si technology is often considered a significant advantage. In view of this, fundamental and applied investigations of various forms of silicon materials maintain their high relevance [2–10]. In particular, the interest in porous silicon (por-Si) is driven by its promising applications in thermo-electrics and microfluidics [11, 12]. Polycrystalline Si (poly-Si) crystals and thin films are the basis of photovoltaics [5, 13, 14] and silicon-on-insulator (SOI) devices [6, 8, 15–18], respectively. Amorphous Si (a-Si) is one of the materials used in sensors [19, 20] and low-cost solar cells [5, 21], photonics [2, 6, 22], and novel microelectronics [6, 14, 23] and radio-electronics applications [24].

Many possibilities for modification of the functional properties of materials, for their advancements in the applications, can be implemented using pulsed laser annealing (PLA) [3, 12, 25–37]. With availability of scanning pulsed laser systems and direct laser writing lithography equipment, investigations of laser modification of materials regain their high relevance for both emerging and well-established semiconductor materials, such as silicon. For example, laser processing has substantially contributed to the advancement of silicon-based solar cells in the last decade [13], enabling efficiencies above 27% (on a single junction cell), which is very close to the intrinsic limit of 29.4% [38]. The compatibility of lasers with mass production and not requiring vacuum conditions has facilitated their introduction into existing industrial cell production lines and offered essential advantages compared to other time-consuming, costly methods of cell structuring. Laser technologies will play a crucial role in developing tandem Si solar cells with perovskites [39].

Raman spectroscopy is generally one of the most often used techniques for characterisation of Si-based functional structures and devices [8, 4, 16, 40–44]. The advantages of Raman spectroscopy in the structural investigation of semiconductors in general and silicon-based structures in particular are better lateral spatial resolution and less probing depth compared to XRD. Moreover, the probing depth is strongly dependent on the wavelength of the excitation laser light (λ_{exc}) and varies from ~10 nm for λ_{exc} = 325 nm to ~10 μm at λ_{exc} = 830 nm [18]. This also applies to microcrystalline Si (mc-Si) and polycrystalline Si (poly-Si) because their optical constants are very close to those of single-crystal Si. Nanocrystalline Si (nc-Si) may have a stronger absorption per unit volume due to the resonance effects, particularly if the band gap increase is caused by the quantum confinement effect in nanocrystals. An intrinsic resonance in Si occurs only at 3.4 eV (364 nm), due to direct gap interband absorption at the Γ point [18]. Amorphous Si (a-Si) is featured by a strong absorption of visible light, thereby reducing the penetration depth of laser excitation by almost an order of magnitude compared to (poly)crystalline Si [45].

In this work, we have used Raman spectroscopy and microscopy to investigate structural modification induced by PLA in amorphous (a-Si) and polycrystalline silicon (poly-Si), Si nanocrystals (NCs) in SiO_2-matrix (ncSi-SiO_2), as well as SiO_2/Si/SiO_2 sandwich structures.

2. Experimental

PLA treatment was performed with the commercially available laser engraver FM-30M-A11-D, equipped with a 30W 1064 nm laser. The laser parameters were the following: spot diameter 10 μm, pulse duration 150 ns, and nominal pulse energy E_{pulse} = 0.75 mJ. During processing, the applied pulse energy was set to 16–22% of E_{pulse}, yielding absorbed fluences of approximately 60230 J·cm^{-2} depending on sample-specific optical absorption. These peak absorbed fluences exceed the melting thresholds by orders of magnitude, consistent with the observed melting/phase–explosion regimes in the scan tracks. By using a set of filters, the laser power density can be tuned in a broad range. Preliminary selection of the regimes suitable for controlled modification of properties of silicon-based materials was performed. Different percentages of the laser power density were used. Other parameters were the following: 50 Hz repetition rate, lane spacing (hatching) 10 μm, scanning speed of 100 or 400 mm/s. Optionally, the sample could be thermally heated to 150°C during PLA, to reduce the drawbacks of the thermal expansion coefficient difference between the film and substrate or between the optically heated part of the samples and the rest of the sample. For each of the chosen PLA regimes, a sample area of 5×5 mm was treated, which enabled reliable registration of the Raman signal from the treated area even without a microscope.

Raman study was performed using the 457 and 830 nm solid-state lasers for excitation, and the spectra were acquired at a single-stage spectrometer MDR-23 (LOMO) or Renishaw 1000, equipped with a TE-cooled CCD detector. To preclude any thermal or photo-induced modification of the samples, the power density of the laser on the sample surface was kept below 10^3 W/cm^2. Raman spectra were recorded at a spectral resolution of 4 cm^{-1}, as proved by the Si phonon peak width of a single-crystal Si substrate. The position of the Si phonon peak at 520.5 cm^{-1} was used as a reference for peak positions in the Raman spectra of the samples. Optical (UV-vis) reflection spectra were obtained using a UV-3600 Plus/UV-3600i Plus spectrometer.

3. Results and discussion

3.1. Raman spectra of the initial samples

Fig. 1 shows typical Raman spectra of initial samples (before PLA) of a-Si, c-Si, Si NCs in SiO_2, and poly-Si. c-Si (used as a reference) exhibits its typical narrow peak at 520 cm^{-1}, with FWHM close to 4 cm^{-1}, which is determined by the spectral resolution of the setup. The poly-Si has a peak with the same FWHM, but its position is shifted by ~0.4 cm^{-1} to higher frequencies. The latter can be caused by a weak compressive stress in the lattice of the poly-Si sample, while the absence of extra peak broadening indicates that the strain is very homogeneous within the grains. No broadening due to size effects is expected, due to μm sizes of the single-crystal domains in poly-Si.

The Raman peak of the nc-Si sample is centered close to the frequency of bulk Si, indicating that the characteristic size of the crystallites is at least tens of nm. The FWHM, larger than 10 cm^{-1}, can be due to the effects related to the high surface-to-volume ratio in NCs, namely, quantum confinement, surface disorder, and inhomogeneous strain. The spectrum of a-Si exhibits a broad band (FWHM ~ 80 cm^{-1}) with a maximum close to 480 cm^{-1}, strongly shifted to lower frequencies compared to c-Si (520 cm^{-1}) due to the bond disorder [4].

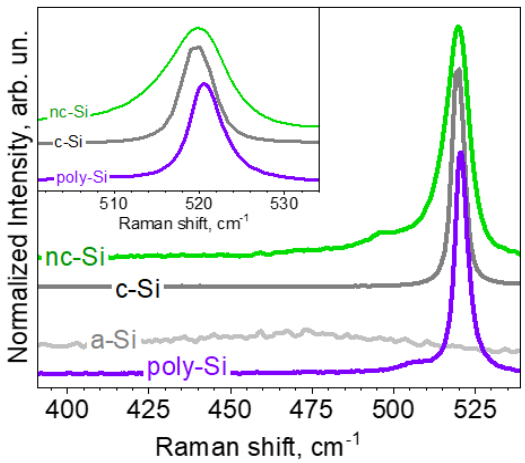

Fig. 1. Typical Raman spectra (λ_{exc} = 457 nm) of the initial samples: amorphous Si (a-Si), SiO_2 film incorporated with Si NCs (ncSi-SiO_2), and polycrystalline Si (poly-Si). A single-crystal Si wafer (c-Si) was measured as a reference. The inset shows the range of the crystalline peak in more detail, highlighting the difference in FWHM and peak position between the spectra.

3.2. Study on the effect of PLA annealing on the structure of the a-Si layer

For a-Si, we have found that PLA with ns-pulsed 1064 nm light in an inert atmosphere leads to the formation of a highly crystalline Si at a certain laser power. This can be seen from the nearly bulk-like position of the Raman peak, 519 cm^{-1}, observed at λ_{exc} = 457 nm for 16% of the maximum PLA power (Fig. 2). Notably, the peak width decreases only by ~1 cm^{-1}, in the sample treated with 19% power, but is significantly narrowed and shifted to 520.5 cm^{-1} at 22% of PLA power. This observation indicates that the PLA-induced crystallization of a-Si is a pronounced threshold process. Comparing the latter spectrum with the reference c-Si spectrum (thin grey line in Fig. 2), one can conclude that the peak position at 520 cm^{-1} corresponds to highly crystalline material with the crystal grain size of tens of nm and a certain value of the compressive strain. The larger FWHM (7 cm^{-1}) compared to c-Si (4 cm^{-1}) can be the result of a moderate quantum confinement and minor strain inhomogeneity.

Furthermore, the asymmetry of the peak at the low-frequency side indicates that even at 22% of the PLA power, the incomplete transformation into large crystallites occurred, and a minor part of the material remains in the form typical for the samples treated at 16% and 19% of the PLA power.

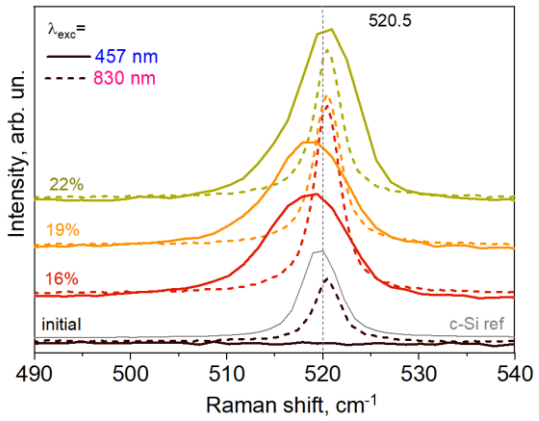

Fig. 2. Raman spectra of PLA-treated a-Si, measured at λ_{exc} = 457 nm (solid lines) and 830 nm (dashed lines). The solid grey line is c-Si at λ_{exc} = 457 nm shown as a reference.

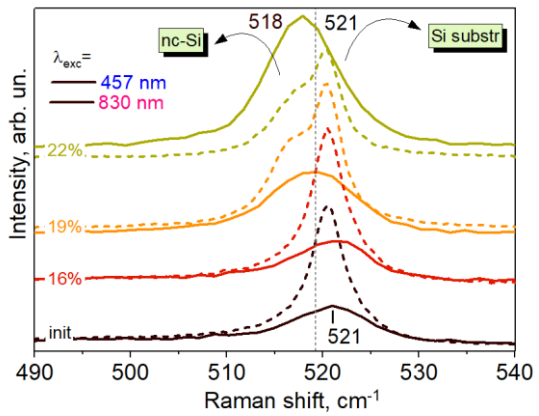

Fig. 3. Raman spectra of PLA-treated SiO_2:Si sample, excited with λ_{exc} = 457 nm (solid lines) and 830 nm (dashed lines).

At λ_{exc} = 830 nm (Fig. 2, dashed curves), the spectra of the initial and all PLA-treated a-Si samples exhibit only a sharp line of single-crystal Si, without noticeable manifestations of the amorphous or nanocrystalline phases. This can be explained by a large penetration depth of this wavelength, ~10 μm, consequently, the Raman signal of the Si substrate dominates the spectrum. In the spectra of the annealed samples, the integral intensity increases by 2-3 times, presumably due to the contribution of the crystallized a-Si layer and deeper penetration of the exciting beam into the substrate.

3.3. Study on the effect of PLA annealing on the structure of the nc-Si layer

For the ncSi-SiO_2 sample, at λ_{exc}= 457 nm, PLA leads to a downward shift of the Raman peak, from 521 to 518 cm^{-1}, without significant narrowing (Fig. 3, solid curves). This can be due to the formation of Si crystallites from small and presumably amorphous Si clusters and free Si ions, present in the initial sample. We can assume that the spectrum of the initial sample is dominated by the signal of the substrate. The efficiency of crystallization increases with increasing PLA power, up to a domination of the signal of crystallites in the spectrum of the sample treated at 22% of PLA power (Fig. 3).

This assumption is confirmed by the inspection of the spectra recorded at λ_{exc} = 830 nm (Fig. 3, dashed curves). At this λ_{exc}, the spectral resolution is higher due to stronger light dispersion in the red than in the blue range. In this case, one can observe two components in the spectra corresponding to 19% and 22% PLA power. Considering that the 830 nm wavelength penetrates much deeper into the Si substrate (~ 5 μm) compared to 457 nm (~ 0.5 μm), the shape of the spectra at λ_{exc} = 830 nm can be explained as follows. For the initial sample, the spectrum differs from the one obtained at λ_{exc} = 457 nm only by a smaller FWHM (due to better dispersion in the red) and stronger intensity (due to deeper penetration in the Si substrate). A similar situation also occurs in the case of 16% of PLA power. For 19% PLA power, a threshold crystallisation was apparently achieved, and λ_{exc} = 830 nm can register its contribution as a Raman line at 518 cm^{-1}. However, a large portion of the 830 nm photons reach the substrate and contribute to the component close to 521 cm^{-1}. At 22% of PLA power, the situation is qualitatively the same, with a slightly larger intensity ratio of the nc-Si band to that of the Si substrate, which is reasonable, because stronger crystallization can occur at 22% compared to 19% power. In the case of λ_{exc} = 457 nm, the difference between the spectra of samples obtained at 19% and 22% of PLA power was more pronounced than at λ_{exc} = 830 nm, which is caused by the domination of the signal from NCs due to stronger absorption of the blue wavelength.

3.4. Study of PLA annealing of poly-Si layer

For poly-Si, we have found that the laser annealing at different intensities and other parameters does not change significantly the position and width of the peaks, but causes a strong variation of the intensity of the Raman peak for $\lambda_{exc} = 830$ nm (Fig. 4).

Moreover, the intensity exhibits even opposite trends in some cases. In the case of the substrate kept at 150 °C, the intensity increases to about one order of amplitude after the treatment at the highest laser power (Fig. 4a). When the substrate is kept at room temperature (and all the other parameters unchanged), no significant change in the intensity is observed (Fig. 4b). Decreasing the scan speed (by factor of 4) results in a gradual and noticeable decrease of the peak intensity (Fig. 4c). Since the position and FWHM of the peak do not change significantly in all three cases, the major reason of the intensity variation and different trends in this variation is not related to the changed crystallinity of poly-Si.

At $\lambda_{exc} = 457$ nm, the peak maximum in the spectrum of the initial poly-Si samples is centered at a much lower frequency, 518 cm^{-1} (spectra not shown), but did not show any significant dependence of the intensity, position, or the lineshape on the PLA power, substrate temperature, or scanning speed. Additional complex investigations are needed to determine the physical reasons for the observed behaviour of the Raman spectra of poly-Si.

3.5. PLA annealing of a-SiO_2 embedded into the Si layer

A perspective application of the PLA of SOI (including SBI – Si between insulator) structures is a method to change their strain to increase the mobility of charge carriers. It is well known that tensile strain in Si layers significantly increases the electron mobility [4, 15, 17, 28]. In case of SOI, local heating and possibly even recrystallization of the Si layer by ultrashort (fs–ns) laser pulses, without noticeable heating of the SiO_2 layer(s), may result in relaxation or elevation of the strain/stress in the Si layer [6, 17]. Below, we demonstrate the results of the PLA treatment of a series of SOI (SBI) structures with different thicknesses of Si and SiO_2 layers.

The scheme of the SiO_2/Si/SiO_2 samples studied in this work is shown in Fig. 5, and the thicknesses of the layers are listed in Table 1. Because the penetration depth of 457 nm light in Si is only ~ 200 nm [18], this ensures that the Raman spectra recorded at λ_{exc}=457 nm originate solely from the embedded Si layer, without contribution from the Si substrate.

Table 1. The thicknesses of the investigated SOI samples according to the notations in Fig. 5.

Sample #	1	2	3	4	5
d_1^{SiO2}, μm	1	1	1.6	1	2
d^{Si}, μm	0.6	0.5	0.25	0.2	0.2
d_1^{SiO2}, μm	0.7	1	1.1	1	1

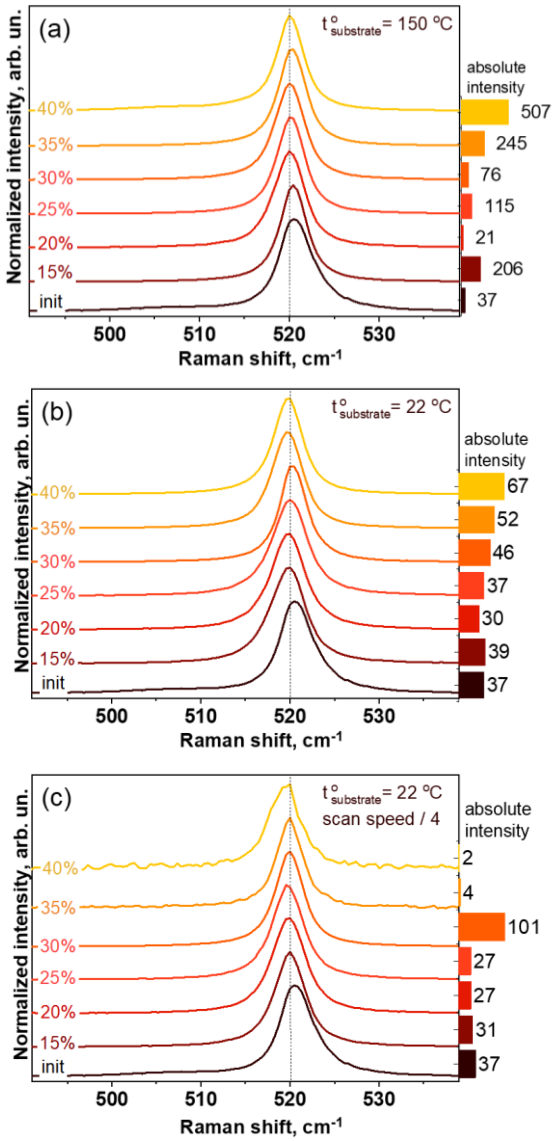

Fig. 4. Normalized Raman spectra of poly-Si samples treated at various laser powers: (a) substrate temperature is 150 °C, (b) substrate temperature is 22 °C, (c) substrate temperature is 22 °C and four times lower scanning speed than that in (b). The absolute intensity of the Raman peaks in each spectrum is indicated by color bars.

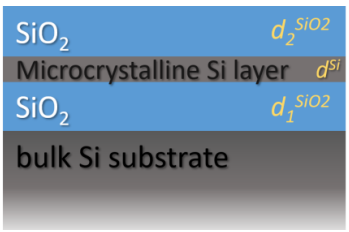

Fig. 5. The scheme of the SiO_2/Si/SiO_2 samples studied in this work. The thicknesses of the layers are listed in Table 1.

Vertical homogeneity of the individual layers was observed using the intensity oscillations in optical reflectance spectra (Fig. 6), which allowed us to calculate the thickness of the layers and verify the values from Table 1.

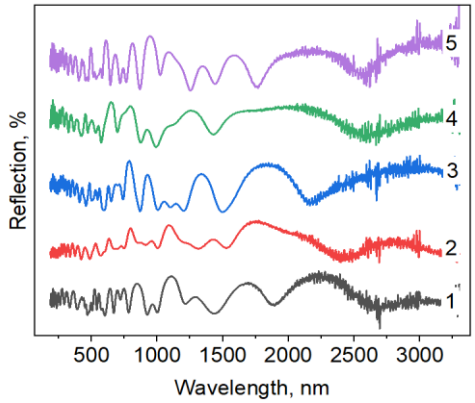

Fig. 6. Optical reflectance spectra of the samples of SiO_2 embedded into the Si layer. The numbers near the curves correspond to the sample numbers in Table 1.

Fig. 7a shows a set of typical Raman spectra of the SOI structure (sample #4), annealed using PLA at various laser powers (P_{PLA}). The spectra of the initial (not annealed) sample and of reference single crystal Si are also shown for comparison. One can see the downward shift of the peak and the increase in its intensity with increasing P_{PLA}.

Because the FWHM does not change significantly, the shift can be caused by the relaxation of compressive strain or the emergence of tensile strain in the Si layer. It is known that due to the difference in the thermal-expansion coefficients of poly-Si and SiO_2, the SiO_2 layer can induce a significant strain in the poly-Si layer, even at the thicknesses equal to several tens to hundreds of nm, and the value of strain can depend on the SiO_2 layer thickness [18].

In Fig. 7b, the dependence of the Raman peak intensity (filled symbols) and frequency position (open symbols) on P_{PLA} is plotted for different samples. From this graph, one can see that different samples have different initial values and different types of dependence. It is worth noting that at the highest P_{PLA}, all the samples tend to have the same values of Raman peak intensity and frequency position, which is indicated by the orange circle. One can assume that the Si layer attains some relaxed state, which is more determined by the power of the light pulses rather than by initial conditions, which vary between the samples.

4. Conclusions

In this work, we have investigated the induced by annealing with a commercial near-infrared scanning ns-pulsed lasers structural modification of amorphous, porous, and polycrystalline silicon, as well as $SiO_2/Si/SiO_2$ multilayer structures by using Raman spectroscopy. For a-Si, we have ascertained that with IR PLA annealing in an inert atmosphere, highly crystalline Si can be obtained at a certain laser power, as inferred from the bulk-like position of the Raman peak, 520.5 cm^{-1}. The formation of Si NCs in the SiO_2 matrix was shown to be a pronounced threshold effect launched within a 1-2% increase in the PLA power. For poly-Si, we have found that the most significant changes in the spectra are a non-monotonic variation of the intensity of the Raman peak, which needs a separate study. The most noteworthy observation for the $SiO_2/Si/SiO_2$ system is that samples with different thicknesses of the SiO_2 and Si layers obtain very close values of the Raman peak intensity after the PLA treatment at the highest power density. This can indicate that PLA annealing drives the crystalline lattice of the embedded Si layer to a more relaxed state, which weakly depends on its thickness and the thickness of both cladding SiO_2 layers. The obtained results demonstrate a high potential of PLA with 1064 nm scanning engraver in tuning the crystallinity and strain state of different allotropes and micro- and nanostructures of silicon.

Acknowledgment

The work was financially supported by the National Research Foundation of Ukraine, grant # 2023.05/0022 for V.M.D., A.A.K., V.V.S., K.V.S., O.V.D.

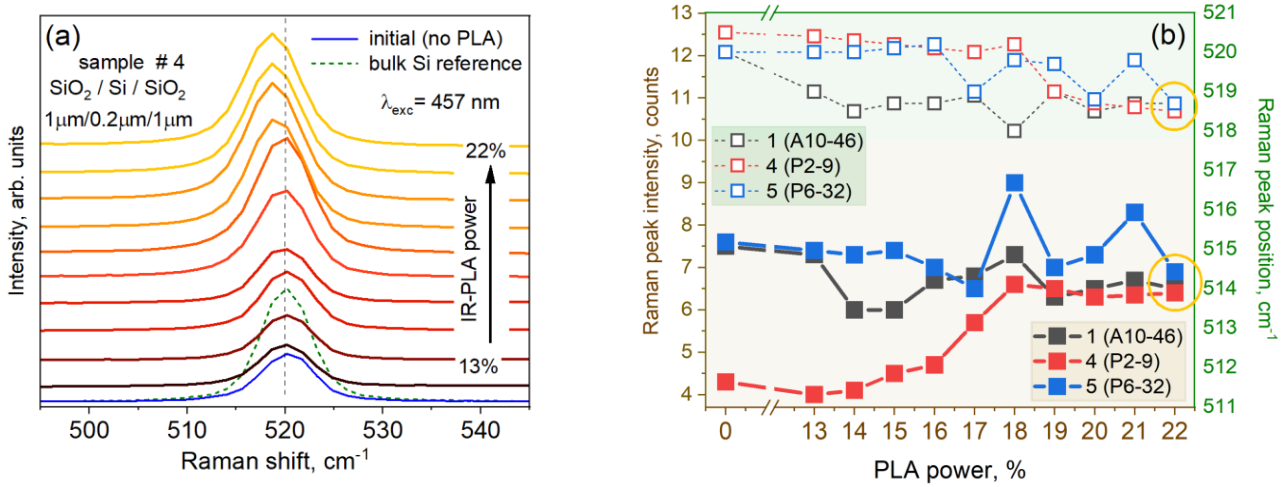

Fig. 7. (a) Typical Raman spectra (λ_{exc} = 457 nm) of $SiO_2/Si/SiO_2$ structure (#4) subject to PLA annealing at various powers. The spectra of the initial sample and the reference single-crystal Si are shown for comparison. (b) Dependence of the Raman peak intensity (filled symbols) and frequency position (open symbols) on P_{PLA} for different samples. The orange circle indicates that at the highest P_{PLA}, all the samples tend to have the same values.

References

1. Xiao Z., Liu W., Xu S. *et al.* Recent progress in silicon-based photonic integrated circuits and emerging applications. *Adv. Optical Mater.* 2023. **11.** P. 2301028. https://doi.org/10.1002/adom.202301028.
2. Tokel O., Turnali A., Makey G. *et al.* In-chip microstructures and photonic devices fabricated by nonlinear laser lithography deep inside silicon. *Nature Photon.* 2017. **11.** P. 639. https://doi.org/10.1038/s41566-017-0004-4.
3. Kryuchyn A., Petrov V., Kosyak I. *et al.* Prospects for creation of the technology of maskless photolithography based on direct laser recording. *SPQEO*. 2024. **28**. P. 93. https://doi.org/10.15407/spqeo28.01.093.
4. Pyo J., Lee B., Ryu H. Evaluation of crystalline volume fraction of laser-annealed polysilicon thin films using Raman spectroscopy and spectroscopic ellipsometry. *Micromachines.* 2021. **12**. P. 999. https://doi.org/10.3390/mi12080999.
5. Zhou J., Su X., Zhang B. *et al.* Ultrafast laser-annealing of hydrogenated amorphous silicon in tunnel oxide passivated contacts for high-efficiency *n*-type silicon solar cells. *Mater. Today Energy*. 2024. **42**. P. 101559. https://doi.org/10.1016/j.mtener.2024.101559.
6. Li J., Wang L., Xu X. *et al.* Local laser annealing for amorphous/polycrystalline silicon hybrid photonics on CMOS. *Opt. Laser Technol.* 2024. **181**. P. 111799. https://doi.org/10.1016/j.optlastec.2024.111799.
7. Michailovska K., Indutnyi I., Shepeliavyi P. *et al.* Luminescent and Raman study of nanostructures formed upon annealing of SiO_x:Sm films. *SPQEO*. 2023. **26**. P. 68. https://doi.org/10.15407/spqeo26.01.068.
8. Yukhymchuk V., Dzhagan V., Valakh M. *et al.* In situ photoluminescence/Raman study of reversible photo-induced structural transformation of nc-Si. *Mater Res. Express.* 2014. **1**. P. 045905. https://doi.org/10.1088/2053-1591/1/4/045905.
9. Khomenkova L., Korsunska N., Torchynska T. *et al.* Defect-related luminescence of Si/SiO_2 layers. *J. Phys: Condens. Matter*. 2002. **14** (48). P. 371. https://doi.org/10.1088/0953-8984/14/48/371.
10. Shi W., Qi D., Wang W. *et al.* Study of femtosecond laser induced periodic structure on amorphous silicon films and crystallization characteristics. *Opt. Laser Technol*. 2025. **181**. P. 111764. https://doi.org/10.1016/j.optlastec.2024.111764.
11. Makukha O., Lysenko I., Belarouci A. Liquid-modulated photothermal phenomena in porous silicon nanostructures studied by μ-Raman spectroscopy. *Nanomaterials*. 2023. **13**. P. 310. https://doi.org/10.3390/nano13020310.
12. Lishchuk P., Belarouci A., Tkach R. *et al.* Impact of thermal annealing on photoacoustic response and heat transport in porous silicon based nanostructured materials. *AIP Conf. Proc.* 2019. **2170**. P. 020008. https://doi.org/10.1063/1.5132727.
13. Fattah T., Chen J., McNab S. *et al.* Nanosecond vs picosecond: the potential for advanced solar cell processing via pulsed laser technology. *J. Appl. Phys.* 2025. **138**. P. 083108. https://doi.org/10.1063/5.0284270.
14. Arduino D., Stassi S., Spano C. *et al.* Silicon and silicon carbide recrystallization by laser annealing: a review. *Materials.* 2023. **16**. P. 7674. https://doi.org/10.3390/ma16247674.
15. Benko T. Design of SOI transistors taking into account the influence of a floating body and a controlled base. *Phys. Chem. Solid State.* 2025. **26**. P. 442. https://doi.org/10.15330/pcss.26.2.442-446.
16. Sasaki N., Takayama S., Sasai R. *et al.* Straight-line-shaped grooves induced by agglomeration in thin Si films obtained by the continuous wave laser crystallization of a-Si on insulator. *J. Electronic Mater.* 2024. **53**. P. 2781. https://doi.org/10.1007/s11664-024-10955-8.
17. Tuyaert R., Scheen G., Aouadi K. *et al.* Post-fab porous silicon in silicon-on-insulator substrates for improved radio frequencies performances. *Mater. Sci. Semicond. Proc*. 2026. **201.** P. 110098. https://doi.org/10.1016/j.mssp.2025.110098.
18. Yoshikawa M., Murakami M., Matsuda K. *et al.* Characterization of Si nano-polycrystalline films at the nanometer level using resonant Raman scattering. *J. Appl. Phys.* 2005. **98**. P. 063531. https://doi.org/10.1063/1.2060954.
19. Mussabek G., Yar-Mukhamedova G., Orazbayev S. *et al.* Silicon nanostructures for hydrogen generation and storage. *Nanomaterials*. 2025. **15**. P. 1531. https://doi.org/10.3390/nano15191531.
20. Ivanov I., Skryshevsky V., Belarouci A. Engineering porous silicon-based microcavity for chemical sensing. *ACS Omega*. 2023. **8**. P. 21265. https://doi.org/10.1021/acsomega.3c02526.
21. Thoma P., Breyer E.T., Thoma O.-M. *et al.* Electrical interface characterization of ultrathin amorphous silicon layers on crystalline silicon. *phys. status solidi (a)*. 2021. **218**. P. 2000079. https://doi.org/10.1002/pssa.202000079.
22. *et al.* Femto-second laser-induced crystallization of amorphous silicon thin films under a thin molybdenum layer. *ACS Appl. Mater. Interfaces.* 2021. **13**. P. 37797. https://doi.org/10.1021/acsami.1c07083.
23. Nayak S., Behravan N., Bisht R. *et al.* Defect-induced density control in amorphous silicon oxide films on 200 mm silicon wafer. *J. Phys. D: Appl. Phys.* 2025. **58**. P. 185308. https://doi.org/10.1088/1361-6463/adc60e.
24. Perrosé M., Baron Y., Lefaucher B. *et al.* Defect engineering for enhanced silicon radiofrequency substrates. *phys. status solidi (a)*. 2024. **221.** P. 2400215. https://doi.org/10.1002/pssa.202400215.
25. Levytskyi S., Cao Z., Koba O. *et al.* Change of the optoelectronic properties of semiconductor compounds induced by nanosecond laser irradiation pulses. *Phys. Chem. Solid State.* 2024. **25**, No 4. P. 892. https://doi.org/10.15330/pcss.25.4.892-902.
26. Petrov V., Kryuchyn A., Beliak Ie. *et al.* Advantages of direct laser writing for enhancing the resolution of diffractive optical element fabrication processes. *Phys. Chem. Solid State.* 2024. **25**, No 3. P. 587. https://doi.org/10.15330/pcss.25.3.587-594.
27. Orhan E., Efil E., Bayram Oz. *et al.* 3D-graphene-laser patterned *p*-type silicon Schottky diode *Mater.*

Sci. Semicond. Proc. 2021. **121** P. 105454. https://doi.org/10.1016/j.mssp.2020.105454.
28. Karlash A., Dmytruk A., Dmitruk I. *et al.* Impact of wavelength, intensity and polarization on the morphology of femtosecond laser-induced structures on crystalline silicon surface. *Appl. Nanosci*. 2022. **12.** P. 1191. https://doi.org/10.1007/s13204-021-01823-6.
29. Gnilitskyi I., Mamykin S., Lanara C. *et al.* Laser nanostructuring for diffraction grating based surface plasmon-resonance sensors. *Nanomaterials*. 2021. **11**. P. 591. https://doi.org/10.3390/nano11030591.
30. García O., García-Ballesteros J., Munoz-Martin D. *et al.* Analysis of wavelength influence on a-Si crystallization processes with nanosecond laser sources. *Appl. Surf. Sci.*. 2013. **278**. P. 214. http://doi.org/10.1016/j.apsusc.2013.01.061.
31. Cheng L., Lv X., Ding D. *et al.* Nanosecond laser annealing processed surface-structured hyperdoped silicon for efficient near-infrared detection. *Nanotechnology*. 2024. **35**. P. 475704. https://doi.org/10.1088/1361-6528/ad6e8d.
32. Garcia-Lechuga M., Casquero N., Siegel J. *et al.* Amorphization and ablation of crystalline silicon using ultrafast lasers: dependencies on the pulse duration and irradiation wavelength. *Laser Photonics Rev.* 2024. **18**. P. 2301327. https://doi.org/10.1002/lpor.202301327.
33. Salman H., Bacıoğlu A., Eken S. Crystallization of hydrogenated amorphous silicon thin film on glass by using ns-pulsed fiber laser operating at 1064 nm. *Mater. Sci. Semicond. Proc*. 2019. **95**. P. 20. https://doi.org/10.1016/j.mssp.2019.02.006.
34. Bouchouri A., Akram M., Øhlckers P. *et al.* Optimization of grayscale lithography for the fabrication of flat diffractive infrared lenses on silicon wafers. *Micromachines*. 2024. **15**. P. 866. https://doi.org/10.3390/mi15070866.
35. Neimash V., Melnyk V., Fedorenko L. *et al.* Tin-induced crystallization of amorphous silicon assisted by a pulsed laser irradiation. *SPQEO*. 2017. **20**. P. 396. https://doi.org/10.15407/spqeo20.04.396.
36. Fedorenko L., Ščajev P., Miasojedovas S. *et al.* Photoluminescent behavior and structural analysis of SnO layers formed by laser-induced oxidation. *Sci. Techn. Adv. Mater*. 2025. **26**. P. 2450213. https://doi.org/10.1080/14686996.2025.2450213.
37. Fedorenko L., Medvids A., Yukhymchuk V. *et al.* Amorphous – Crystalline phase transition in nano-structural thin SiO_x layers induced by pulsed laser radiation. *Opt. Laser Technol*. 2022. **148**. P. 107526. https://doi.org/10.1016/j.optlastec.2021.107526.
38. Wu H., Ye F., Yang M. *et al.* Silicon heterojunction back-contact solar cells by laser patterning. *Nature* 2024. **635**. P. 604. https://doi.org/10.1038/s41586-024-08110-8.
39. Rodkey N., Kaal S., Sebastia-Luna P. *et al.* Pulsed laser deposition of $Cs_2AgBiBr_6$: From mechano-chemically synthesized powders to dry, single-step deposition. *Chem. Mater.* 2021. **33**, No 18. P. 7417. https://doi.org/10.1021/acs.chemmater.1c02054.
40. Pylypova O., Antonin S., Fedorenko L. *et al.* Influence of laser annealing of silicon enriched SiO_x films on their electrical conductivity silicon. *Silicon.* 2022. **14**. P. 12599. https://doi.org/10.1007/s12633-022-01959-2.
41. Korsunska N., Bulakh B., Jumayev B. *et al.* Raman scattering characterization of macro- and nano-porous silicon. *Appl. Surf. Sci*. 2005. **243.** P. 30. https://doi.org/10.1016/j.apsusc.2004.06.151.
42. Neimash V., Goushcha A., Shepeliavyi P. *et al.* Self-sustained cyclic tin induced crystallization of amorphous silicon. *J. Mater. Res.* 2015. **30**, No 2. P. 3116. https://doi.org/10.1557/jmr.2015.251.
43. Roisin N., Colla M.-S., Raskin J.P., Flandre D. Raman strain–shift measurements and prediction from first-principles in highly strained silicon. *J. Mater. Sci.: Mater. Electron*. 2023. **34**. P. 373. https://doi.org/10.1007/s10854-022-09769-3.
44. Bayat P., Vogel D., Rodriguez R.D. *et al.* Thermo-mechanical characterization of copper through-silicon vias (Cu-TSVs) using micro-Raman spectroscopy and atomic force microscopy. *Microelectron. Eng.* 2015. **137**. P. 101–104. http://doi.org/10.1016/j.mee.2015.02.004.
45. Carpenter III J.V., Bailly M., Boley A. *et al.* Substrate-independent analysis of microcrystalline silicon thin films using UV Raman spectroscopy. *phys. status solidi (b)*. 2017. **254**. P.1700204. https://doi.org/10.1002/pssb.201700204.

Authors' contributions

Dzhagan V.M.: conceptualization, writing – review & editing, project administration.
Lytvyn P.M.: conceptualization, formal analysis.
Korchovyi A.A.: methodology, data curation.
Yukhymchuk V.O.: data curation, formal analysis.
Strelchuk V.V.: data curation, formal analysis.
Svezhentsova K.V.: writing – review & editing.
Androsyuk G.M.: validation.
Dubikovsky O.B.: investigation, visualization,
Dzhahan V.V.: investigation, visualization.
Kondratenko S.V.: conceptualization.

Authors and CV

Volodymyr M. Dzhagan, Dr.Sci., Prof., Acting Deputy Director of ISP NASU. Authored over 200 papers. Expertise: optical and vibrational properties of semiconductors, nano- and composite materials.
E-mail: dzhagan@isp.kiev.ua,
https://orcid.org/0000-0002-7839-9862

Petro M. Lytvyn, PhD, Head of Department at ISP NASU. His research focuses on solid-state physics, functional materials, nanophysics of semiconductors and related materials. Author over 350 peer-reviewed publications, 10 patents, 9 monographs.
E-mail:plyt2007@gmail.com,
https://orcid.org/0000-0002-0131-9860

Andrii A. Korchovyi, PhD, Senior Researcher at the Laboratory for scanning probe microscopy, ISP NASU. Authored over 100 papers. Expertise: atomic force microscopy, semiconductor materials and nanostructures. E-mail: akorchovyi@gmail.com, https://orcid.org/0000-0002-8848-7049

Volodymyr O. Yukhymchuk, Prof., Dr.Sci., Head of Optics and spectroscopy Dpt., ISP NASU. Authored over 300 publications. Expertise: optical and vibrational spectroscopy, Raman scattering, SERS, plasmonics, luminescence, semiconductors, nanostructures. E-mail: v.yukhymchuk@gmail.com, https://orcid.org/0000-0002-5218-9154

Viktor V. Strelchuk, Prof. Dr.Sci., Leading Researcher at the Laboratory of submicron optical spectroscopy, ISP NASU. Authored over 300 publications, 10 patents, 6 textbooks. Expertise: physics of semiconductors, Raman and PL spectroscopy of semiconductors and nanostructures.
E-mail: viktor.strelchuk@ccu-semicond.net, https://orcid.org/0000-0002-6894-1742

Galyna M. Androsiuk, Researcher at ISP NASU. The area of her scientific interests is nanomaterials and methods of their investigations.
E-mail: androsiuk.g@gmail.com

Kateryna V. Svezhentsova, PhD, Senior Researcher at ISP NASU. Authored over 50 publications. Field of researches: physics and technology of semiconductor materials, IR and THz detectors.
E-mail: sveshentsova@ukr.ua
https://orcid.org/0000-0002-4309-556X

Oleksandr V. Dubikovskyi, PhD in Physics and Mathematics, Researcher at the Department of Ion-Beam Engineering, ISP NASU. Authored above 20 papers. Expertise: ion-beam modification and mass-spectrometry of semiconductor structures.
E-mail: dubikovsky_o@ukr.net
https://orcid.org/0000-0002-1504-8440

Vladyslav V. Dzhahan, Bachelor student of the Faculty of Physics, Taras Shevchenko National University of Kyiv. Research interests: optical spectroscopy, molecular physics, nanostructures, sensors. Authored 1 research paper. E-mail: dzhahan.vlad@knu.ua, https://orcid.org/0009-0009-7046-9086

Sergiy V Kondratenko, Prof., Dr.Sci., Dean of the Faculty of Physics, Kyiv Taras Shevchenko National University. Expertise: physics of semiconductors, nanoelectronics and photovoltaics. Authored more than 80 papers.
E-mail: kondratenko@knu.ua, http://orcid.org/0000-0002-4403-7732

Раманівське дослідження структурних змін у кремнієвих матеріалах, викликаних скануванням ІЧ-наноімпульсним лазером

В.М. Джаган, П.М. Литвин, А.А. Корчовий, В.О. Юхимчук, В.В. Стрельчук, К.В. Свеженцова, Г.М. Андросюк, О.В. Дубіковський, В.В. Джаган, С.В. Кондратенко

Анотація. Зі зростанням доступності скануючих імпульсних лазерних систем та обладнання для літографії прямого лазерного запису дослідження лазерної модифікації матеріалів знову набувають великої актуальності як для нових, так і для добре відомих напівпровідникових матеріалів, таких як кремній. У даній роботі за допомогою Раманівської спектроскопії досліджено структурну модифікацію аморфного (a-Si) та полікристалічного кремнію (poly-Si), нанокристалів Si в матриці SiO_2 (ncSi-SiO_2), а також багатошарових SiO_2/Si/SiO_2 структур, відпалених імпульсним лазерним випромінюванням при 1064 нм (ІЛВ) за допомогою комерційного скануючого лазера (гравера). Спектроскопія Раманівського розсіювання була використана як основний метод дослідження індукованих лазером структурних змін, завдяки високій чутливості параметрів фононних піків до структурного розупорядкування та механічного напруження решітки. Порівняння спектрів, виміряних при різних довжинах хвилі збудження, дозволяє досліджувати відпалені структури на різній глибині. Для a-Si імпульсний лазерний відпал спричинює локальне формування висококристалічних включень. Для набору SiO_2/Si/SiO_2 багатошарових зразків з різними комбінаціями товщин шарів, ІЛВ приводить до релаксації в стан, який далі не залежить від товщини Si та SiO_2 шарів.

Ключові слова: лазерний відпал, аморфний кремній, полікристалічний кремній, Si нанокристали.